Hittite Journal of Science and Engineering, 2021, 8 (1) 27–33
ISSN NUMBER: 2148–4171
DOI: 10.17350/HJSE19030000209

# Corrosion Behavior of Graphene Nanoplatelet-Coated $TiB_2$ Reinforced AZ91 Magnesium Matrix Semi-Ceramic Hybrid Composites

**Engin Cevik, Murat Gundogan, Alper Incesu, Muhammet Emre Turan**
Karabuk University, Department of Metallurgical and Materials Engineering, Karabuk, Turkey

**ABSTRACT**

In this study; Hybrid composites containing different proportions of $TiB_2$ and graphene were produced using the pressure infiltration method. Inert SF6 gas is used to prevent oxidation in the productions. While 8 bar infiltration pressure was provided by argon gas, the infiltration temperature was chosen as 800°C. The corrosion behaviors of the composite materials were examined. Corrosion resistance was determined by potentiodynamic and immersion corrosion testing in 3.5% NaCl solution. In addition, SEM examinations were conducted to understand the corrosion mechanisms. At the end of the measurements, the highest porosity was measured as %4,7 in composite containing 1% graphene compared to pure matrix and composite containing only TiB2. The added reinforcement (TiB2 and Graphene) elements cause decreases in corrosion resistance. The highest corrosion resistance was achieved in AZ91 alloys.

***Article History:***
*Received: 2020/09/26*
*Accepted: 2021/02/10*
*Online: 2021/03/31*

***Correspondence to**: Engin Cevik, Karabuk University, Metallurgical and Materials Engineering, 78000, Karabük, TURKEY*
*E-Mail: engincevik@karabuk.edu.tr*

**Keywords:**
Graphene, AZ91, $TiB_2$, Magnesium matrix composites, Corrosion.

## INTRODUCTION

Recent environmental protection policies focus on the need to reduce the weight of vehicles in order to increase fuel efficiency and reduce the impact of greenhouse gases emission [1]. Magnesium stands out as the structural metal in cases where weight reduction is important for materials used in industry and vehicles [2]. Low density, good strength to weight ratio, better heat dissipation, acceptable damping capacity, machinability, and recyclability make magnesium a much more attractive structural metal compared to steel and aluminum [2–4]. Despite all these superior properties, high corrosion rate in aggressive environments, relatively low absolute strength, and elastic modulus when compared to other metallic structural materials are the most important unfavorable properties of magnesium alloys [2,5–7].

One way to produce high strength, corrosion-resistant magnesium alloys is the production of Mg-based composites by the addition of reinforcement particles such as ceramics [7]. Reinforcement of Mg matrix composites (MMCs) with suitable ceramic particles such as SiC, TiC, and $TiB_2$ can exhibit high specific strength and acceptable corrosion resistance when the correct combination of reinforcement and a light metal matrix is used [8]. Properties of magnesium matrix such as corrosion resistance, wear resistance, hardness can be developed with Ti-based ceramic particles (TiC, TiAlC, and $TiB_2$ reinforcement [8–10]. For magnesium matrix composites, $TiB_2$ is a highly compatible reinforcing element because the crystal structures of the two are compatible with each other as a hexagonal closed pack (HCP).

Another method to increase strength and corrosion resistance is the addition small amount of nano-sized particles with high surface area (such as carbon nanotube and graphene) to the magnesium matrix also causes significant increases in mechanical properties and corrosion resistance of composite [11–14]. Say et al. [15] determined that AZ61 and AZ91 matrix composites reinforced with lower CNTs (0.1 wt.% or 0.2 wt.%) and non-reinforced alloy had better corrosion resistance than composites reinforced with higher CNTs (0.5 wt.%). Similarly, Munir et al. [16] reported that Mg–Graphene nanoplatelets (GNP) composites were reinforced with 0.1 wt.% GNP showed the best corrosion resistance in the same corrosion environment as compared to the pure Mg.

**Table 1.** Chemical composition of AZ91 (wt %).

| Alloy | Mg | Al | Fe | Mn | Ni | Zn | COST-231 Hata |
|---|---|---|---|---|---|---|---|
| AZ91 | 89,9 | 9 | 0,005 | 0,33 | 0,002 | 0,7 | -23,7 |

In this study, graphene nanoplatelet-coated $TiB_2$ was added to AZ91 magnesium alloy to see the effect of both $TiB_2$ ceramic particles and high surface area graphene on the corrosion properties of AZ91 matrix composites. Four different AZ91 matrix composites containing graphene and $TiB_2$ in different ratios were produced by the pressure infiltration method for the first time to the best of our knowledge. Corrosion characteristics of produced composites were investigated comparatively.

## MATERIAL AND METHODS

High purity (99,9 %) graphene nanoplates and $TiB_2$ particles (99,95 % purity) were used as reinforcement materials in this study and commercial AZ91 alloy, the chemical composition of which is given in Table 1, was used as the matrix element. The first stage is the preparation of reinforcement materials. At this stage, the graphene doping process to TiB2 particles with an average particle size of 45 microns was performed using the vacuum distillation method.

Graphene nano-plates were added into ethyl alcohol in the proportions given in Table 2 and the graphene-ethanol suspension was formed by mixing in the ultrasonic bath. After that, $TiB_2$ particles were added in determined proportions (Table 2) and mixed during 15 minutes. Then, the alcohol in the suspension evaporated from the vacuum distillation at 200°C on the magnetic stirrer. As a result, $TiB_2$ particles containing three different ratios of graphene were produced.

**Table 2.** Volume (%) contents of the produced samples.

| Composites | Volume Fraction (%) | | |
|---|---|---|---|
| | $TiB_2$ | GNP | AZ91 |
| S1 | 0 | 0 | 100 |
| S2 | 50 | 0 | 50 |
| S3 | 49,75 | 0,25 | 50 |
| S4 | 49,5 | 0,5 | 50 |
| S5 | 49 | 1 | 50 |

The second stage is the preparation of preforms. 7 mm inner diameter and 350 mm length 316L quality stainless tubes, which are shown in Fig. 1, are used as preform holders. The end of the stainless tube is covered with an alumina filter with 85% porosity. Preforms with a length of Ø7x50 mm were prepared by hand vibrating in a stainless tube so that the reinforcement ratio was 50%. The preform was covered

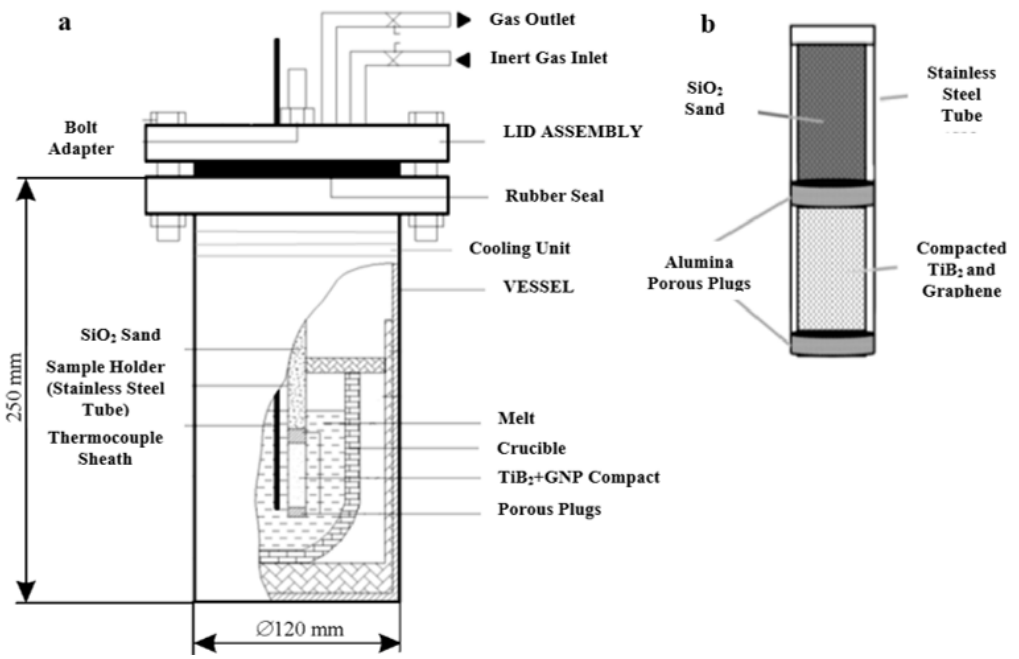


**Figure 1.** Schematic view of the assembly (a) diagram of the stainless steel tube specimen holder (b).

with an alumina filter and the remaining part of the tube was filled with silica cast sand in order to provide the homogeneous distribution of particles during infiltration.

Finally, the AZ91 alloy we prepared in a 600 gr capacity crucible was placed in the assembly and the cover of the assembly was closed using a plastic gasket. Later, the furnace was raised to 800°C, which is determined as the infiltration temperature, and kept for 1 hour in order to ensure complete melting. Sf6 gas was passed through the assembly to provide an inert gas environment for production.

The preform in a stainless tube was immersed in the melt and kept for 2 minutes for the liquid metal to reach its temperature. Finally, 8 bar infiltration pressure was applied with argon gas and left for 2 minutes, then argon gas was released from the unit. After the composites were produced, they were removed from the infiltration unit. The stainless tubes were cleaned from the surface with a lathe and the composites were obtained.

In order to bring the produced composite materials to the desired dimensions, they were cut with a diamond disc cutting device. The grinding process was applied with an automatic machine from coarse to fine (240-1200 mesh SiC) grits and then the polishing process was completed with 3 µm and 0.3 µm alumina.

SEM images were taken on the Carl Zeiss Ultra Plus Gemini Fesem device. XRD analysis of prepared composite samples was performed at 40 kV generator voltage, 30 mA current in the range of 20° -90°, and with a scanning step of 0.02.

Experimental density measurement was carried out according to the Archimedes principle. The theoretical density was measured by the mixture principle and % porosity amounts were determined by both of using these data.

Two different corrosion tests were applied to composite specimens, namely potentiodynamic and immersion types of corrosion. A potentiodynamic polarization test was carried out in PARSTAT 4000 device in a 3.5% NaCl solution. The composite specimens prepared were molded in bakelite with open front and back for holding. Thanks to the holder prepared before, the samples were placed in the device and the tests were carried out. A pair of graphite rods were used as counter electrodes and a saturated calomel electrode (SCE) was used as a reference electrode for free corrosion potential measurements. Tests were carried out at room temperature. To determine the open circuit (OC) value in the tests, -400 mV was applied to the samples for 900 seconds by 1 mV/s scan rate. As a result of the tests, the corrosion rate in mm/year was calculated using Faraday's law with the following formula;

$$CR = 3{,}27x10^{-3}\, x\, I_{corr}\, x(EW)\,/\,d \qquad (1)$$

CR: corrosion rate (mm/year),
$I_{corr}$: corrosion current density (µA/cm$^2$),
EW: equivalent weight (gr) and
d: density (gr/cm$^3$).

Composite samples prepared for immersion tests were first weighed with precision scales. Then, the polymer net was dipped into the mixture prepared with distilled water containing 3.5% NaCl in a glass jar at room temperature. The composite samples were taken out of the glass jar in 3,6,12,24 hours and cleaned for 5 minutes with the help of distilled water, and then weighed with a precision scale after cleaning with alcohol and drying. After weighing, the samples were put back into the polymer net and immersed in the solution in the glass jar and the measurements were made again at the specified hours. At the end of 24 hours, surface images were taken from the samples with an EDS attached to an SEM microscope. At the end of the test, corrosion behavior was determined depending on the amount of graphene added, taking into account the weight loss.

## RESULTS AND DISCUSSION

Doped graphene nanoplatelets to $TiB_2$ particles with Van Der Waals bonds was achieved with the vacuum distillation process. SEM photographs of $TiB_2$ particles that do not contain graphene and 1% graphene doped $TiB_2$ reinforcement are shown in Fig. 2. Although it is seen in partial agglomerations, it can be said that graphene nanoplatelets are attached successfully to the surface of the $TiB_2$ particle.

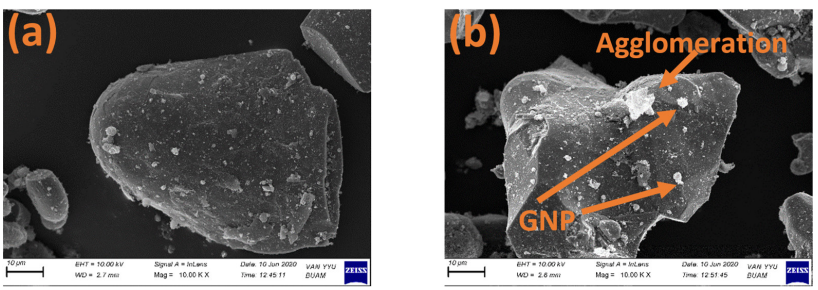


**Figure 2.** SEM images of GNP added $TiB_2$ powders a) 0% and b) 1%.

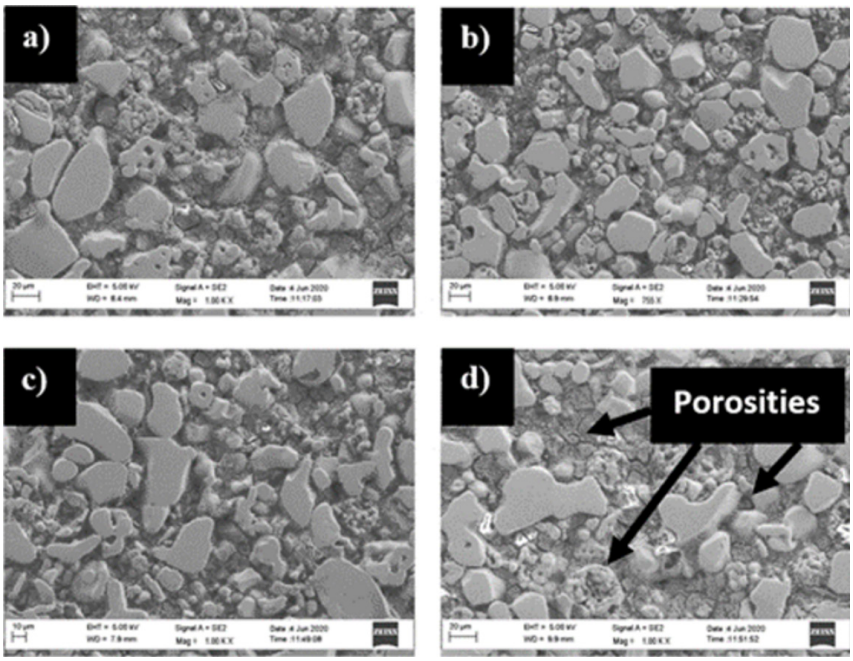


**Figure 3.** a) AZ91+$TiB_2$, b) 0.25% GNP+AZ91+$TiB_2$ c) 0.5% GNP+AZ91+$TiB_2$ and d) 1% GNP+AZ91+$TiB_2$.

The microstructure images of the produced hybrid composites are given in Fig. 3. Unlike other composite production methods, the pressure infiltration method makes it possible to produce with high reinforcement elements [17]. For example, while the powder metallurgy production method can reach a maximum of 30% by volume, it is observed that agglomeration in the structure increases and porosity reaches unacceptable levels at higher reinforcement rates [18]. When hybrid composites produced with 50% particle reinforcement are evaluated fabricated by pressure infiltration method, it can be deduced that homogeneous particle distribution is achieved successfully in all graphene ratios. However, as the proportion of graphene in the structure increased, the amount of porosity increased by 5% compared to non-graphene reinforced composites due to the adverse effect of wettability between the reinforcement and the matrix (Table 3) [19-20].

With liquid metal infiltration, it has been observed that liquid metal diffusion occurs even between particles that are very close to each other. This result shows that the infiltration process is successful despite the very high reinforcement content and that the strong interaction between the reinforcement and matrix can be fully achieved. However, micro-cracks can be attributed to the differences in the cooling rate between the reinforcement and the matrix materials are occurred.

**Table 3.** Density and porosity results of produced samples.

| *Sample Code* | *Theoretical Density* | *Actual Density* | *Porosity* |
|---|---|---|---|
| *S2* | *3,165* | *3,035* | *4,10742* |
| *S3* | *3,159* | *3,012* | *4,65337* |
| *S4* | *3,153* | *3,005* | *4,69394* |
| *S5* | *3,148* | *3,00001* | *4,70108* |

Fig. 4 shows the XRD analyzes made on the composite samples. When X-ray diffractions are analyzed, the $Al_{12}Mg_{17}$ compound is detected in the matrix element [8]. In the produced composites, the $TiB_2$ phase is observed in addition to the magnesium and $Al_{12}Mg_{17}$ phases. Furthermore, there is no extra peak and this situation shows that no phase formation occurs during the production phase due to the interaction of the reinforcement and the matrix.

The corrosive properties of the composites were investigated in a 3.5% NaCl solution. The potentiodynamic po-

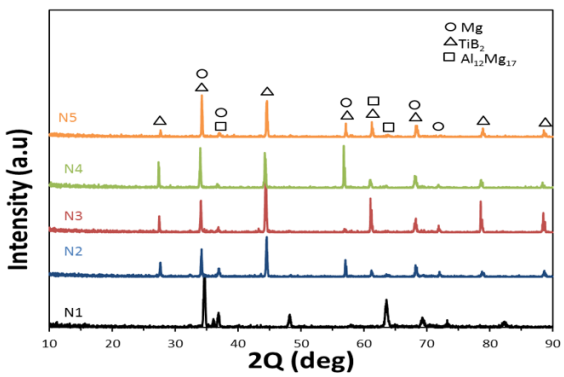


**Figure 4.** XRD analysis results of fabricated composites.

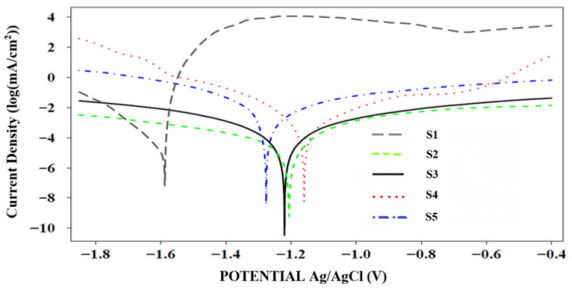


**Figure 5.** Potentiodynamic polarization test charts.

larization test was performed separately in the anodic and cathodic regions (Scanning Interval: -0.4 V vs. Ag / AgCl to -1.85 V vs. Ag / AgCl) and the results are shown in Fig. 5.

Composites with $TiB_2$ reinforced AZ91 matrix exhibits higher $I_{corr}$ values than an unreinforced alloy (Table 4). This can be attributed to the galvanic coupling between the reinforcement phase and the magnesium matrix. The matrix element acts as the anode while the reinforcing element acts as the cathode. For this reason, a very rapid reaction occurs in the first place and this process continues until the anode is exhausted. The fact that the reinforcement phase did not pass into the solution but settled to the bottom during the experiment.

Corrosion ($E_{corr}$) values were obtained at the end of the 15 min. open circuit test. Corrosion rates which are calculated with Faraday's law of produced samples are presented in Table 4.

Considering the corrosion rate (CR) and icorr (CCD) values given in Table 4, the lowest corrosion rate is observed in the S1 coded sample. The highest corrosion rate can be seen in the sample coded S5. As a result of the analysis made on Tafel curves, the ceramic reinforcement made dramatically reduces the corrosion resistance of the metal matrix. Reinforcement materials such as SiC, $TiB_2$ are known as inert materials because they act as inert electrodes. When a metal of sufficient conductivity forms a galvanic couple, it leads to the formation of a corroded surface very quickly [21].

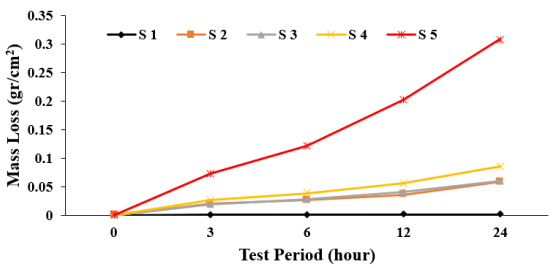


**Figure 6.** Immersion corrosion results in 3.5% NaCl.

The galvanic coupling formed between TiB2 reinforcement and the AZ91 matrix increased significantly with the addition of graphene to the structure and accelerated the corrosion of the matrix. As it is known, potentiodynamic tests are generally performed in very short periods. In order to support these results, immersion corrosion tests were carried out in the same environment.

The results of the immersion corrosion test conducted for 24 hours support the potentiostat tests. As shown in Fig. 6, it has been observed that all composite types exhibit lower corrosion resistance compared to the AZ91 matrix. However, the most noteworthy part here is the great decrease in corrosion resistance after the addition of graphene. This decrease reached its maximum levels with the addition of 1% graphene. This is due to the galvanic coupling that occurs between the matrix and the reinforcement. On the other hand, it is thought that increasing porosity amounts with the addition of graphene have a negative effect on corrosion resistance and increase crevice corrosion [22,23,24].

When immersion test results are evaluated, remarkable detail is that the slopes of the mass loss-time graph of magnesium matrix composites consist of two different regions. Namely, an increase is observed in the slope of the graphs after the first 6 hours in all samples. The reason for this can be thought to be the corrosive solution moves into the sample and increases the corrosion rate.

$TiB_2$ particles, which remain stable with the dissolution of the matrix element, separate from the structure and collapse to the bottom when they are disconnected from the matrix, which causes the loss of mass to increase more than expected [23].

**Table 4.** Potentiodynamic polarization test results.

| *Specimen* | *Surface Area ($cm^2$)* | *CC (μA)* | *CCD (μA / $cm^2$)* | *CR (mm / year)* | *$E_{corr}$ (V)* |
|---|---|---|---|---|---|
| *S1* | *0.283* | *2.10* | *7.42* | *0.16* | *-1.59* |
| *S2* | *0.283* | *9.14* | *32.30* | *0.40* | *-1.21* |
| *S3* | *0.283* | *19.87* | *70.21* | *0.88* | *-1.02* |
| *S4* | *0.283* | *36.94* | *130.53* | *1.63* | *-1.16* |
| *S5* | *0.283* | *80.43* | *284.20* | *3.55* | *-1.28* |

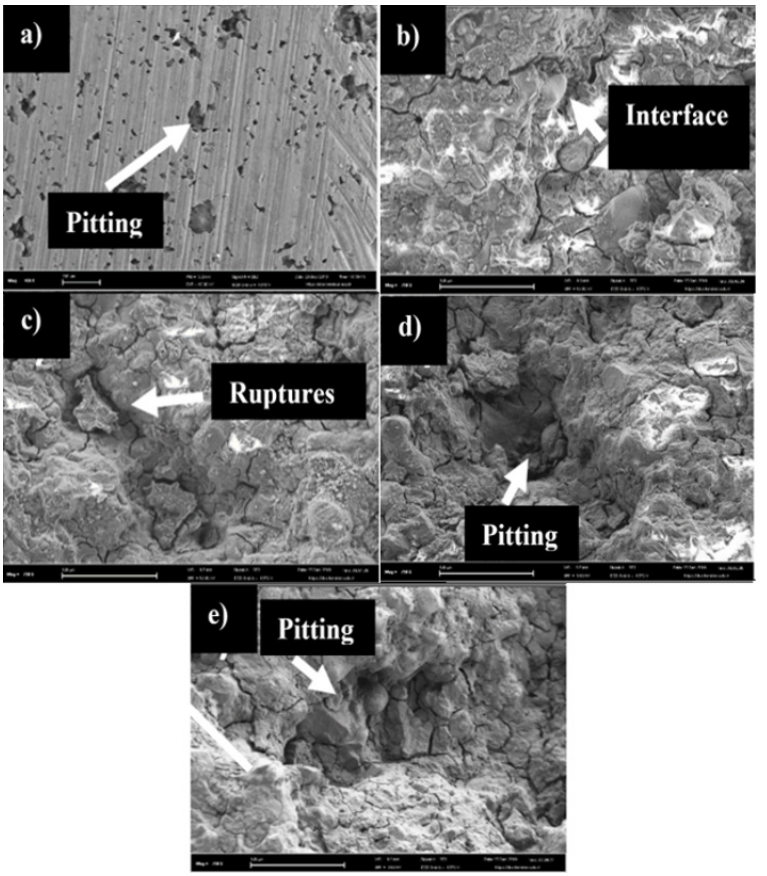


**Figure 7.** SEM analysis a) AZ91, b) AZ91+$TiB_2$, c) AZ91+$TiB_2$+%0,25 GNP, d) AZ91+$TiB_2$ +%0,5 GNP, e) AZ91+$TiB_2$ +%1 GNP after immersion tests.

In Fig. 7, corroded surface photographs of the examined composite materials are shown. When SEM photographs of the corroded surface are examined, it can be seen that the aggressive solution environment where the pitting potential increases with the addition of both $TiB_2$ and graphene causes higher mass loss. Corrosion that started at the matrix and reinforcement interface resulted in the dissolution of the surrounding matrix element by the $TiB_2$ particles acting as cathodes and the particles detached from the structure during the experiment.

## CONCLUSION

In this study, different ratios of graphene and $TiB_2$ reinforced composite materials with the AZ91 matrix were produced by the pressure infiltration method. Corrosion tests were carried out for all samples produced. As a result of this study;

a) As a result of the metallographic examination, it was observed that the TiB2 reinforcement element was homogeneously distributed in composite reinforcement materials.

b) According to the density measurement, the porosity ratio increased with the increasing graphene ratio.

c) When potentiodynamic and immersion corrosion tests are examined, it has been that the corrosion resistance decreases as the reinforcement element increases. Generally, the corrosion mechanism in the structure has been determined as pitting and crevice corrosion.

## ACKNOWLEDGMENT

This study was supported by the Scientific Research Projects Coordination Unit of Karabuk University within the scope of the project numbered KBÜ-BAP-18-YL-110.

### References

1. Ramalingam VV, Ramasamy P, Kovukkal MD, Myilsamy G. Research and development in magnesium alloys for industrial and biomedical applications: a review. Met. Mater. Int. (2019) 1–22.
2. Mingo B, Arrabal R, Mohedano M, Pardo A, Matykina E. Corrosion, and wear of PEO coated AZ91/SiC composites. Surf. Coat. Technol. 309 (2017) 1023–1032.
3. Luo AA. Materials comparison and potential applications of magnesium in automobiles. in: Essent. Read. Magnes. Technol., Springer, pp. 25–34, 2016.
4. Wang XM, Wang XJ, Hu XS, Wu K, Zheng MY, Processing, microstructure, and mechanical properties of Ti6Al4V particles-reinforced Mg matrix composites. Acta Metall. Sin. Engl. Lett. 29 (2016) 940–950.
5. Razavi M, Fathi MH, Meratian M. Microstructure, mechanical

properties, and bio-corrosion evaluation of biodegradable AZ91-FA nanocomposites for biomedical applications. Mater. Sci. Eng. A. 527 (2010) 6938–6944.
6. Razavi M, Fathi M, Savabi O, Razavi SM, Heidari F, Manshaei M, Vashaee D, Tayebi L. In vivo study of nanostructured diopside (CaMgSi2O6) coating on magnesium alloy as biodegradable orthopedic implants. Appl. Surf. Sci. 313 (2014) 60–66.
7. Song J, She J, Chen D, Pan F. Latest research advances on magnesium and magnesium alloys worldwide. J. Magnes. Alloys. (2020).
8. Gobara M, Shamekh M, Akid R, Improving the corrosion resistance of AZ91D magnesium alloy through reinforcement with titanium carbides and borides. J. Magnes. Alloys. 3 (2015) 112–120.
9. Jiang QC, Li XL, Wang HY. Fabrication of TiC particulate reinforced magnesium matrix composites. Scr. Mater. 48 (2003) 713–717.
10. Sahoo BN, Panigrahi SK. Synthesis, characterization, and mechanical properties of in-situ (TiC-TiB2) reinforced magnesium matrix composite. Mater. Des. 109 (2016) 300–313.
11. Du X, Du W, Wang Z, Liu K, Li S. Ultra-high strengthening efficiency of graphene nanoplatelets reinforced magnesium matrix composites. Mater. Sci. Eng. A. 711 (2018) 633–642.
12. Xiang SL, Gupta M, Wang XJ, Wang LD, Hu XS, Wu K. Enhanced overall strength and ductility of magnesium matrix composites by low content of graphene nanoplatelets. Compos. Part Appl. Sci. Manuf. 100 (2017) 183–193.
13. Rashad M, Pan F, Hu H, Asif M, Hussain S, She J. Enhanced tensile properties of magnesium composites reinforced with graphene nanoplatelets. Mater. Sci. Eng. A. 630 (2015) 36–44.
14. Turan ME, Sun Y, Akgul Y. Mechanical, tribological and corrosion properties of fullerene reinforced magnesium matrix composites fabricated by semi powder metallurgy. J. Alloys Compd. 740 (2018) 1149–1158.
15. Say Y, Guler O, Dikici B. Carbon nanotube (CNT) reinforced magnesium matrix composites: The effect of CNT ratio on their mechanical and corrosive properties. Mater. Sci. Eng. A. (2020) 139636.
16. Munir K, Wen C, Li Y. Graphene nanoplatelets-reinforced magnesium metal matrix nanocomposites with superior mechanical and corrosion performance for biomedical applications. J. Magnes. Alloys. (2020).
17. Candan E, Ahlatci H, Cimenoglu H. Abrasive wear behaviour of Al–SiC composites produced by pressure infiltration technique. Wear. 247 (2001) 133-138.
18. Aydın F, Sun Y, Ahlatci H, Turen Y. Investigation of Microstructure, Mechanical and Wear Behaviour of B4C Particulate Reinforced Magnesium Matrix Composites by Powder Metallurgy. Trans. Indian Inst. Met. 71 (2018) 873-882.
19. Kavımani V , Prakashi KS and Thankachan T. Investigation of graphene-reinforced magnesium metal matrix composites processed through a solvent-based powder metallurgy route. Department of Mechanical Engineering, Anna University Regional Campus, Coimbatore 641 046, India, 2019.
20. Sun X, Li C, Dai X, Zhao L, Li B, Wang H, Liang C, Li H, Fan J. Microstructures and properties of graphene-nanoplatelet-reinforced magnesium-matrix composites fabricated by an in situ reaction process, J.Alloys Compd. 835 (2020) 155125.
21. Zakaria, HM. Microstructural and corrosion behavior of Al/SiC metal matrix composites. Ain Shams Engineering Journal. 5 (2014) 831-838.
22. Turhan MC, Li Q, Jha H, Singer RF, Virtanen S. Corrosion behavior of multiwall carbon nanotube/magnesium composites in 3.5% NaCl. Electrochşimica Acta. 56 (2011) 7141-7148.
23. Turan ME, Sun Y, Akgul Y, Turen Y, Ahlatci H.The effect of GNPs on wear and corrosion behaviors of pure magnesium. J.Alloys Compd. 724 (2020) 14-23.
24. Rashad M, Fusheng Pan F, Asif M, Chen X. Corrosion behavior of magnesium-graphene composites in sodium chloride solutions. J. Magnes. Alloys. 5 (2017) 271-276.